Check for updates

View Article Online
View Journal

Dalton Transactions

An international journal of inorganic chemistry

Accepted Manuscript

This article can be cited before page numbers have been issued, to do this please use: J. Wenger, W. J. Rowe and M. Mehta, *Dalton Trans.*, 2026, DOI: 10.1039/D6DT00986G.

This is an Accepted Manuscript, which has been through the Royal Society of Chemistry peer review process and has been accepted for publication.

Accepted Manuscripts are published online shortly after acceptance, before technical editing, formatting and proof reading. Using this free service, authors can make their results available to the community, in citable form, before we publish the edited article. We will replace this Accepted Manuscript with the edited and formatted Advance Article as soon as it is available.

You can find more information about Accepted Manuscripts in the Information for Authors.

Please note that technical editing may introduce minor changes to the text and/or graphics, which may alter content. The journal's standard Terms & Conditions and the Ethical guidelines still apply. In no event shall the Royal Society of Chemistry be held responsible for any errors or omissions in this Accepted Manuscript or any consequences arising from the use of any information it contains.

ROYAL SOCIETY OF CHEMISTRY

rsc.li/dalton

View Article Online
DOI: 10.1039/D6DT00986G

ARTICLE

Activation of N_2O, CO_2, and CO at a sterically protected phosphorus center

Received 00th January 20xx,
Accepted 00th January 20xx

DOI: 10.1039/x0xx00000x

John S. Wenger,*[a] William J. Rowe,[a] and Meera Mehta*[a]

Functionalization of a sterically encumbered phosphorus precursor enables varied activation pathways for N_2O, CO_2, and CO. The potasssium phosphanide salt, [K(crypt)][(M^{s}FluInd*)PH] (crypt = 2.2.2.cryptand; M^{s}FluInd* = a sterically demanding hydrindacenyl substituent), was synthesized and treated with either N_2O or $^{13}CO_2$ to afford the potassium phosphinate, [K(crypt)][(M^{s}FluInd*)PHO$_2$], or the potassium phosphacarboxylate, [K(crypt)][(M^{s}FluInd*)PH(^{13}CO$_2$)], respectively. Deprotonation of the TMS-functionalized (TMS = trimethylsilyl) phosphine, (M^{s}FluInd*)PTMSH, followed by treatment with either N_2O or $^{13}CO_2$ resulted in the formation of a phoshanorcaradiene, (M^{s}FluInd*)P, and an arylphosphaketene, (M^{s}FluInd*)P^{13}CO, respectively. Reversible CO binding at phosphorus allows for the interconversion between (M^{s}FluInd*)P and (M^{s}FluInd*)PCO. The mechanism for the formation of (M^{s}FluInd*)PCO from (M^{s}FluInd*)P and CO was investigated computationally.

Introduction

The reactivity of low-valent phosphorus species is currently under intense investigation to access new avenues in small-molecule activation.[1] Reactivity patterns between functionalized phosphorus reagents and N_2O are now well-established.[2] Typically, N_2O reacts as an O-atom transfer reagent to form highly stable P–O bonds with the generation of either free N_2 or N_2-capture products.[3] Alternatively, the N_2O molecule may remain intact in the formation of P–N bonded adducts.[2, 4]

Phosphaketenes represent a versatile class of molecular synthons, and previously reported arylphosphaketenes, (Mes*)PCO (Mes* = 2,4,6-tri-*tert*-butylphenyl) and (^{Dipp}Ter)PCO (^{Dipp}Ter = 2,6-bis(2,6-diisopropylphenyl)-phenyl) were synthesized *via* O-atom abstraction from CO_2 by functionalized phosphorus precursors, (Mes*)PTMS$_2$ and (^{Dipp}Ter)PGaCp* (Cp* = pentamethylcyclopentadiene), respectively (Figures 1A, 1B).[5]

The formation of phosphaketenes by direct CO activation has also been observed.[6] The sterically encumbered monomeric (phosphino)phosphinidene, **P^{Ar**}** (Ar** = 2,6-bis[di(4-tert-butylphenyl)methyl]-4-methylphenyl), binds CO at the terminal, monovalent P atom to form the (phosphino)phosphaketene, **P^{Ar**}CO**, which engages in metallomimetic ligand-exchange reactions and loses CO *via* photolysis to form the precursor, **P^{Ar**}** (Figure 1C).[1a-c]

Sterically demanding hydrindacenyl substituents, such as M^{s}FluInd*, have gained popularity to access highly reactive, unsaturated main group compounds (Figure 1D).[7] Notably, the hydrindacenyl phosphanorcaradiene, (M^{s}FluInd^{tBu})P, was shown to engage in molecular-strain induced, phosphinidene reactivity in the activation of small molecules, including isocyanides, which represent isoelectronic analogues of CO (Figure 1D).[1d]

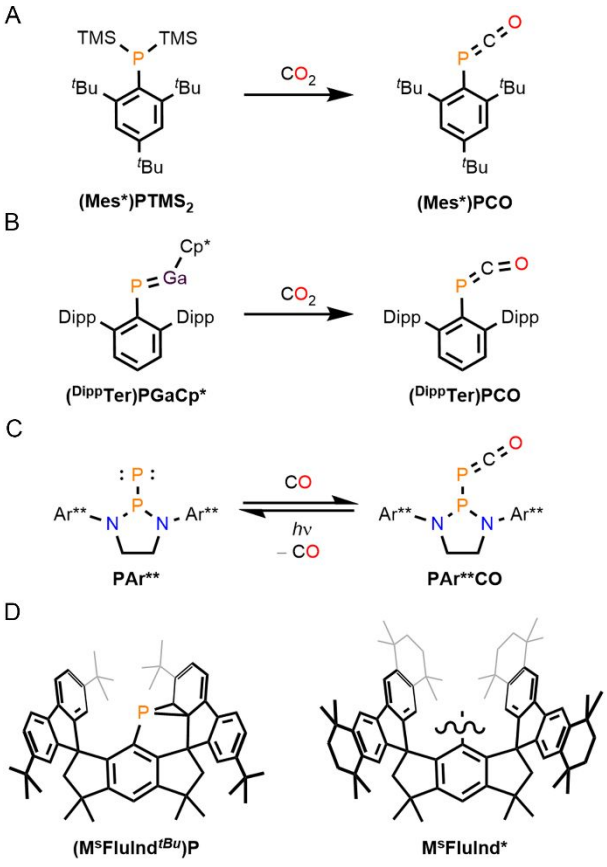

Figure 1. Synthesis of (A) (Mes*)PCO, (B) (^{Dipp}Ter)PCO, and (C) **P^{Ar**}CO**. (D) Depictions of (M^{s}FluInd^{tBu})P and the hydrindacenyl ligand M^{s}FluInd*.

[a] Department of Chemistry, University of Oxford, 12 Mansfield Road, Oxford, OX1 3QR, U.K. john.wenger@chem.ox.ac.uk, meera.mehta@chem.ox.ac.uk

Open Access Article. Published on 29 April 2026. Downloaded on 4/30/2026 5:17:44 AM.
This article is licensed under a Creative Commons Attribution 3.0 Unported Licence.

Dalton Transactions Accepted Manuscript

View Article Online
DOI: 10.1039/D5DT00986C

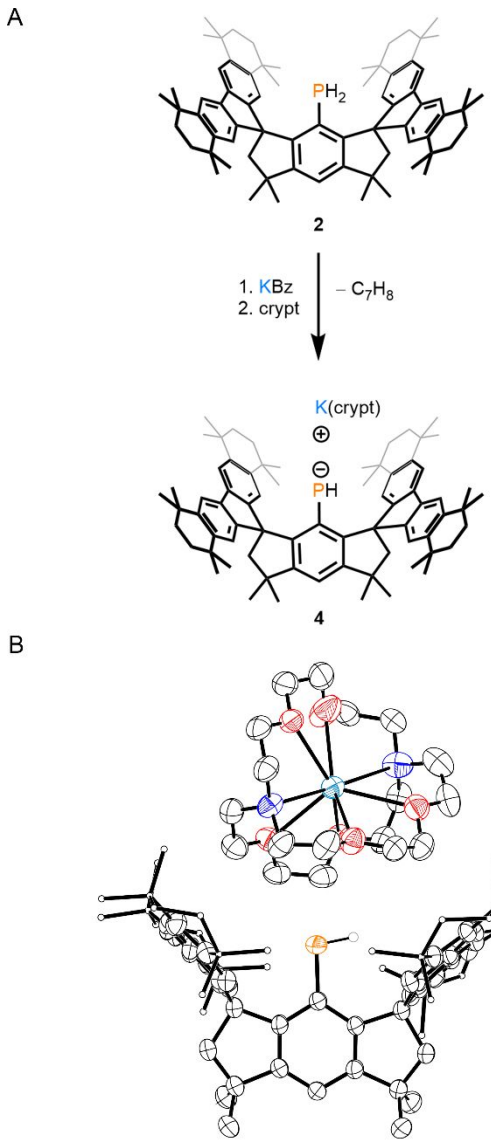

Figure 2. (A) Synthesis of **4**. (B) Thermal ellipsoid plot (50% probability) of **4**. C-bound H atoms and disordered components are omitted for clarity. Select C atoms and H atoms are shown as spheres of arbitrary radius for clarity. Color code: P orange, O red, C black, H grey, K teal, N blue.

We recently reported the sterically encumbered hydrindacenyl phosphines, (M^{s}FluInd*)PCl$_2$ (**1**), (M^{s}FluInd*)PH$_2$ (**2**) and (M^{s}FluInd*)PTMSH (**3**), which were employed as precursors in the first syntheses of thermally robust arylhalodiphosphenes, (M^{s}FluInd*)PPX (X = Cl, Br, I).[8] We rationalized that compounds containing an anionic phosphorus site within the sterically protected environment created by the M^{s}FluInd* ligand could activate gaseous small molecules.

Herein, we report the isolation of the primary phosphanide, [K(crypt)][(M^{s}FluInd*)PH] (**4**). In the presence of excess N_2O or $^{13}CO_2$, compound **4** forms either the oxidation product, [K(crypt)][(M^{s}FluInd*)PHO$_2$] (**5**), or the $^{13}CO_2$-captured product, [K(crypt)][(M^{s}FluInd*)PH($^{13}CO_2$)] (^{13}**6**), respectively. In contrast, when compound **3** is reacted with potassium benzylate before being treated with N_2O or $^{13}CO_2$, the phosphanorcaradiene, (M^{s}FluInd*)P (**7**), or the arylphosphaketene, (M^{s}FluInd*)P^{13}CO (^{13}**8**), are obtained, respectively. Compound **7** is quantitatively converted to (M^{s}FluInd*)PCO (**8**) in the presence of CO gas under mild conditions, and photolysis of compound **8** results in the formation of compound **7** *via* the elimination of CO.

Results and Discussion

Compound **4** was synthesized by treatment of compound **2** with potassium benzylate followed by crypt in benzene (Figure 2A). Crypt was included in the reaction mixture to efficiently sequester the K cation from the primary phosphanide and to facilitate the isolation of **4** as a crystalline salt. Fully sequestered, or "naked", primary phosphanide anions remain rare and often require multiple equivalents of crown ether to synthesize.[9] Recrystallization from a mixture of tetrahydrofuran (THF)/pentane afforded dark-green crystals of **4**•(THF)(pentane)$_{0.5}$ in a 77% yield. ^{31}P NMR analysis of the product reveals a doublet resonating at –69.9 ppm with a $^1J_{PH}$ value of 154 Hz. Single-crystal X-ray diffraction (SC-XRD) analysis of **4** confirms the sequestration of the K cation and no P–K interaction (Figure 2B). The P–C bond length in **4** is 1.788(2) Å and is significantly shorter than that of **2** [1.8424(15) Å], consistent with delocalization of a P-centered lone pair into the hydrindacenyl substituent.[8] Furthermore, the M^{s}FluInd* ligand in **4** appears to adopt a more open conformation relative to **2** to accommodate the {PH} and {K(crypt)} units. The centroid–centroid distance between the five-membered rings of the fluorenyl substituents in **4** [6.8513(17) Å] is greater than that of **2** [6.5460(7) Å].[8]

Treatment of **4** with an excess of N_2O results in the formation of **5** in an 86% yield (Figure 3A). The ^{31}P NMR spectrum of **5** features a single doublet resonating at 1.2 ppm with a large $^1J_{PH}$ coupling constant of 476 Hz, consistent with the presence of a phosphinate anion.[10] SC-XRD analysis of the product confirms the presence of two P-bound O atoms, indicating that the P(I) center of **4** had been oxidized by two equivalents of N_2O to form a pentavalent phosphorus species (Figure 3B). The {PHO$_2$} motif in **5** does not coordinate the K cation and is disordered about two positions, which precludes much meaningful discussion about crystallographic metrics. Notably, the centroid–centroid distance between the five-membered rings of the fluorenyl substituents in **5** [6.9134(16) Å] is greater than that of **4**, consistent with the presence of the larger {PHO$_2$} motif.

When **4** is treated with 1 atm of $^{13}CO_2$ at room temperature, the $^{13}CO_2$ capture-product ^{13}**6** is generated *in situ* (Figure 3A). Despite attempts to perform the reaction under rigorously dry conditions, compound **2** is also observed in the reaction mixture, which we suggest arises by the protonation of **4** by adventitious water. The ^{31}P{^{1}H} NMR spectrum of ^{13}**6** features a singlet at –85.5 ppm. The ^{13}C{^{1}H} NMR spectrum similarly exhibits a prominent singlet associated with the isotopically labelled ^{13}C atom at 168.0 ppm. We suggest that dynamic

Open Access Article. Published on 29 April 2026. Downloaded on 4/30/2026 5:17:44 AM.
This article is licensed under a Creative Commons Attribution 3.0 Unported Licence.

Dalton Transactions Accepted Manuscript

This journal is © The Royal Society of Chemistry 20xx

Please do not adjust margins

View Article Online
DOI: 10.1039/D6DT00986G

Open Access Article. Published on 29 April 2026. Downloaded on 4/30/2026 5:17:44 AM.
This article is licensed under a Creative Commons Attribution 3.0 Unported Licence.

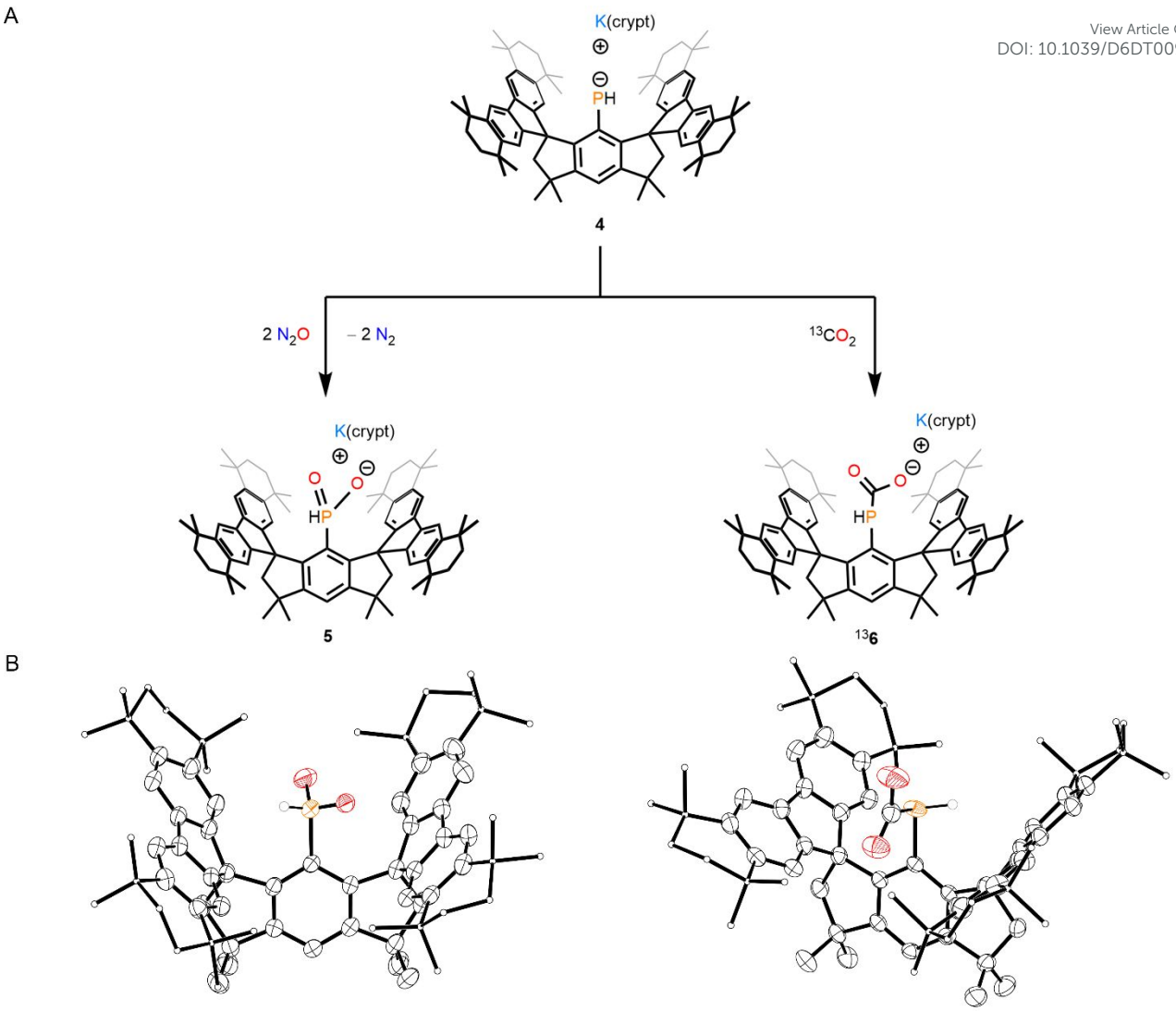

Figure 3. (A) Synthesis of **5** and ^{13}**6**. (B) Thermal ellipsoid plots (50% probability) of **5** (*left*) and ^{13}**6** (*right*). C-bound H atoms, disordered components, and counter cations are omitted for clarity. Select C atoms and H atoms are shown as spheres of arbitrary radius for clarity. Color code: P orange, O red, C black, H grey.

interaction between the ^{13}C-bound O atoms and the sequestered K cation in solution results in the broadening of the ^{31}P and ^{13}C NMR resonances, such that the $^{1}J_{PC}$ coupling is not observed. SC-XRD analysis of ^{13}**6** confirms the formation of the P–$^{13}CO_2$ bond, with a bond length of 1.906(2) Å, and coordination of the {PH$^{13}CO_2$} motif to the K cation in the solid state, with an O–K bond length of 2.741(2) Å (Figure 3B). The P–C_{aryl} bond length is 1.827(2) Å, and the C–P–^{13}C bond angle is 104.41(10)°. The formation of the O–K bond seemingly necessitates a relatively open conformation of the M^{s}FluInd* unit to accommodate the {K(crypt)} cation, and the centroid–centroid distance between the five-membered rings of the fluorenyl substituents in ^{13}**6** is 6.9296(13) Å. Further, a high-resolution electrospray ionization mass spectrometry experiment clearly identified the isotopically labelled anion, ^{13}**6**–K$^-$ (^{13}**6**–K$^-$ refers to the anion formed upon loss of the K cation from ^{13}**6**). Compound ^{13}**6** was found to be unstable and could not be separated from the decomposition product, **2**.

Next, we investigated the TMS-functionalized phosphine, **3**, as a precursor for analogous reactions involving N_2O and CO_2. Treatment of **3** with KBz followed by N_2O results in the formation of **7** in a 59% yield (Figure 4A). ^{1}H and ^{13}C{^{1}H} NMR spectra of **7** appear complex, consistent with the desymmetrization of the M^{s}FluInd* backbone. The ^{31}P{^{1}H} NMR spectrum of **7**, however, features a single resonance at –153.0 ppm (Figure 5A). SC-XRD analysis of **7**•(toluene)$_{0.5}$ confirms its identity as a hydrindacenyl phosphanorcaradiene, with similar structural characteristics to the literature-known species, (M^{s}FluInd^{tBu})P (Figure 4B).[1d] However, the central P atom is disordered across two positions, precluding much meaningful discussion of bond metrics. In this preparation of **7**, N_2O is activated by the elimination of KOTMS and N_2 along with dearomatization of a fluorenyl substituent by the resulting low-coordinate P atom. Compound **7** was also prepared independently by treatment of **1** with two equivalents of KC_8, in an 81% yield, following an adapted literature protocol.[1d]

Dalton Transactions Accepted Manuscript

Please do not adjust margins

View Article Online
DOI: 10.1039/D6DT00986G

Open Access Article. Published on 29 April 2026. Downloaded on 4/30/2026 5:17:44 AM.
This article is licensed under a Creative Commons Attribution 3.0 Unported Licence.

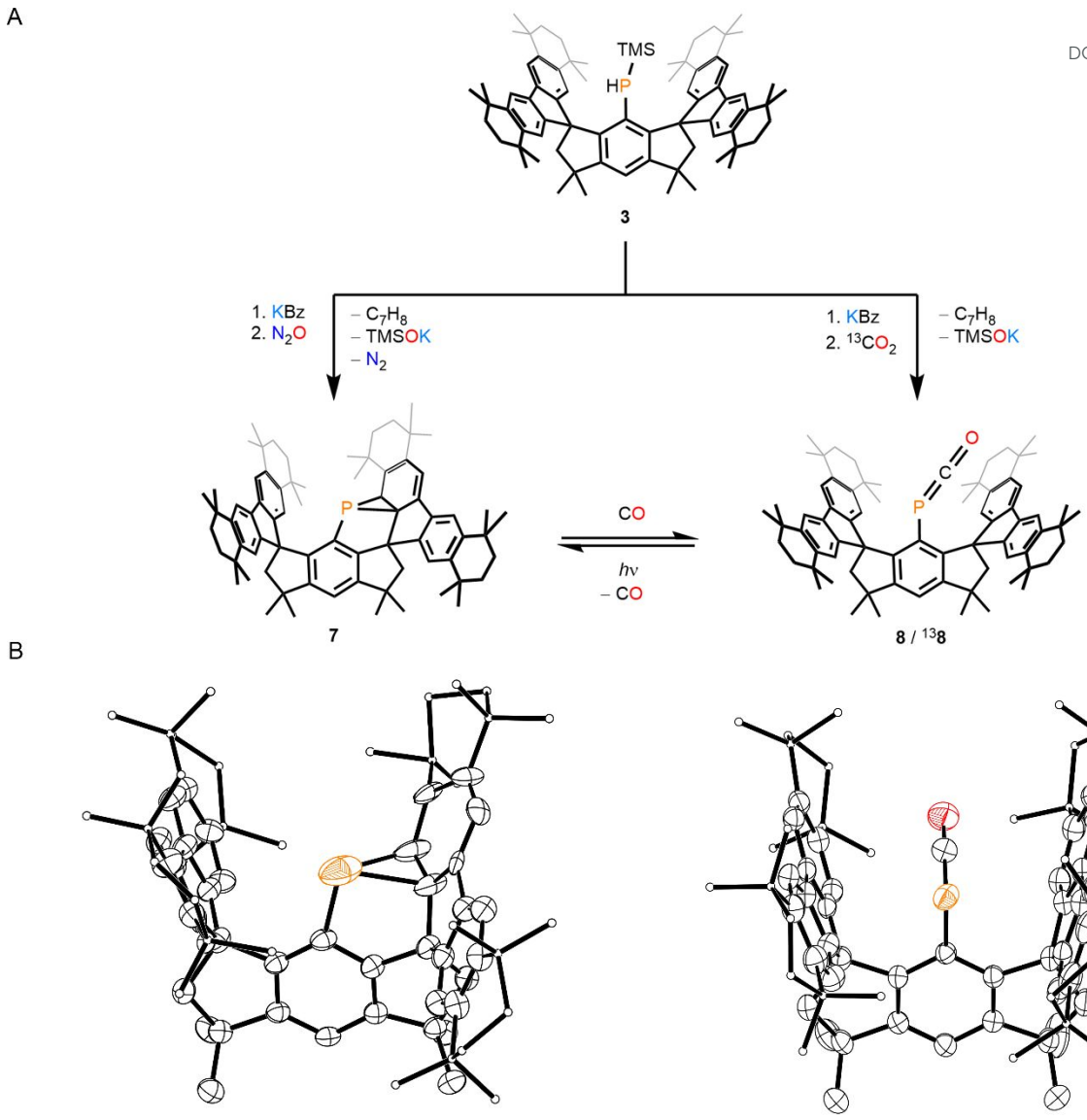

Figure 4. (A) Synthesis of **7**, **8**, and ^{13}**8**. (B) Thermal ellipsoid plots (50% probability) of **7** (*left*) and ^{13}**8** (*right*). C-bound H atoms, disordered components, and counter cations are omitted for clarity. Select C atoms are shown as spheres of arbitrary radius for clarity. Color code: P orange, O red, C black.

We exposed compound **7** to 1 atm of CO at 50 °C overnight to form the arylphosphaketene, **8**, *in situ* (Figure 4A). ^{1}H and ^{13}C{^{1}H} NMR spectra of **8** reveal a symmetrical M^{s}FluInd* environment. The ^{31}P NMR spectrum of **8** features a characteristic resonance at –233.1 ppm (Figure 5A), and the ^{13}C{^{1}H} NMR spectrum of **8** features a doublet at 203.0 ppm with a $^{1}J_{PC}$ coupling constant of 113 Hz. The IR spectrum of **8** features a strong band at 1948 cm^{-1} associated with the carbonyl stretch of the {PCO} unit (Figure 5B). Crystals of ^{13}**8** (*vide infra*) were grown from a concentrated mixture of hexane/toluene and feature crystallographic disorder of the {PCO} motif about two positions (Figure 4B). In ^{13}**8**, the M^{s}FluInd* motif adopts a more closed conformation relative to **4**, **5**, or ^{13}**6**, and features a lower centroid–centroid distance between the five-membered rings of the fluorenyl substituents of 6.1909(14) Å.

Exposure of **8** to 390 nm light for 2 h results in nearly quantitative conversion back to **7** (Figure 4A, Supplementary Figure S42).[5c] Despite working under dark conditions, we were unable to isolate **8** as a pure bulk material due to rapid decomposition to form **7** during workup procedures.

We exposed a reaction mixture containing KBz and **3** to 1 atm of $^{13}CO_2$ (Figure 4A). The resulting solution contains a major product with spectral data that match those of **8**, but with the expected variations arising from ^{13}C enrichment at the phosphaketene motif, and we assign these signals to ^{13}**8**. The ^{31}P nucleus of ^{13}**8** resonates as a doublet in the ^{31}P NMR spectrum and the coupled resonance in the ^{13}C NMR spectrum appears with dramatically enhanced intensity (Figure 5A). The reaction mixture containing ^{13}**8** was stripped of solvent and the IR spectrum of the resulting solid residue features a carbonyl stretch at lower wavenumber than **8** at 1911 cm^{-1} (Figure 5B), as expected.

In a prior report, transition-state calculations for the activation of substrates including an alkene, alkyne, and silane by (M^{s}FluInd^{tBu})P revealed a reaction mechanism in which concerted breaking of the PC_2 ring with the activation of the

This journal is © The Royal Society of Chemistry 20xx

Dalton Transactions Accepted Manuscript

Please do not adjust margins

View Article Online
DOI: 10.1039/D6DT00986G

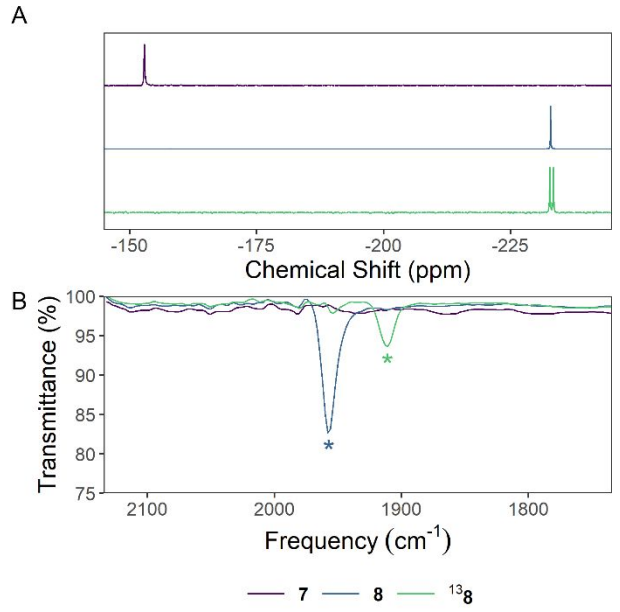

Figure 5. Stacked (A) $^{31}P\{^{1}H\}$ NMR spectra and (B) IR spectra of **7**, **8**, and ^{13}**8**. Signals in the IR spectra assigned to a carbonyl C–O bond stretching mode are denoted with an asterisk.

C═C, C≡C, or Si–H bonds, respectively.[1d] In contrast, activation of an amine by (M^{s}FluInd^{tBu})P proceeded through the breaking of the PC_2 ring upon coordination of the amine to the P center, followed by activation of the N–H bond.[1d] To build on these previous insights, we investigated the reaction mechanism for the formation of **8** from **7** and CO computationally. A simultaneous, two-dimensional relaxed surface scan (r^{2}SCAN-3c) was performed, in which the P–C1 (C1 refers to the carbonyl carbon) bond was extended and the P–C3 (C3 refers to a C atom in a fluorenyl group) bond was contracted, starting from the theoretical coordinates for **8** (Figure 6A, Supplementary Figures S44-45). The optimized coordinates obtained near the maximum of the scanned potential energy surface were used as an input for a transition-state search, which identified the transition state, **TS** (Figure 6A). The ΔG of formation of **TS** is 16.4 kcal/mol higher than that of the starting materials and 37.7 kcal/mol higher than that of **8**.

Topological analysis (X2C-PBE0-D3BJ/x2c-TZVPPall//r^{2}SCAN-3c) of the electron density (ρ) of **TS** identified (3, –1) critical points along the P–C1 and P–C2 interatomic vectors (Figure 6B), and no bond critical point along the P–C3 interatomic vector.[11] Inspection of the Laplacian of ρ ($\nabla^2\rho$) of **TS** in the plane defined by the P, C1, and C3 atoms finds negative values along the P–C2 interatomic vector, consistent with the presence of a covalent bonding interaction (Figure 6B). The P–C1 bonding region does not feature similar continuity of negative values and is consistent with dative interactions between the P and C1 atoms.

Natural bond orbital (NBO) analysis (PBE0-D3BJ/def2-TZVP//r^{2}SCAN-3c) of **TS** identified a C1-centered lone pair and P–C2 and P–C3 bonding and antibonding orbitals (Supplementary Figure S46, Supplementary Table S7). Second order perturbation theory (E^2) analysis reveals delocalization of electron density from the P–C3 bonding orbital into a vacant *p*-

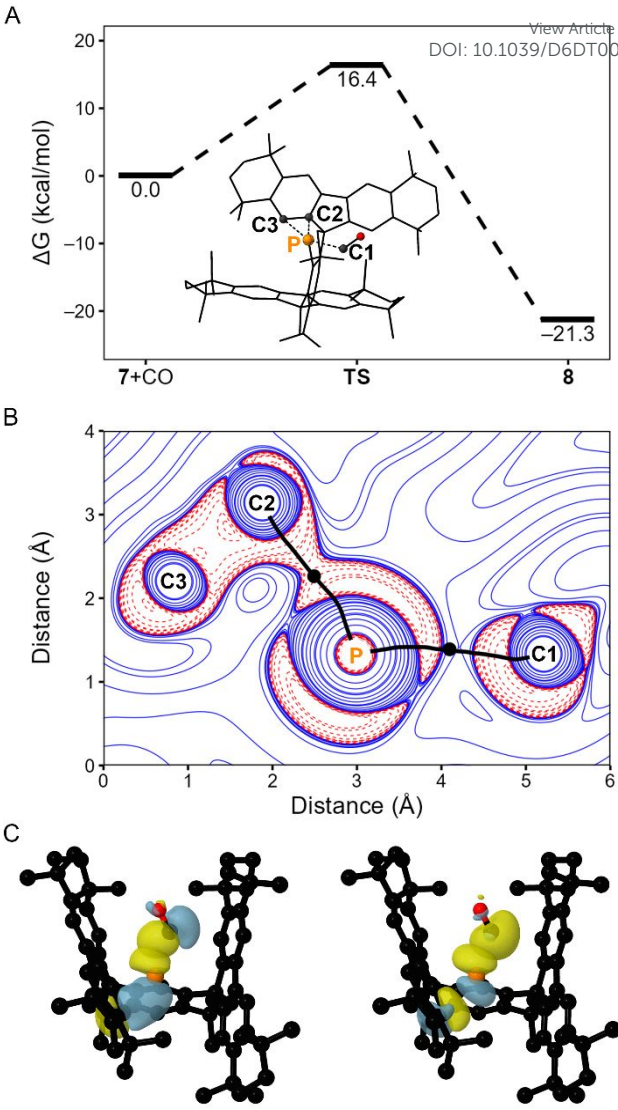

Figure 6. (A) Gibbs free energy profile (r^{2}SCAN-3c) for the synthesis of **8** from **7** and CO *via* transition state, **TS**. A ball-and-stick diagram of **TS** is shown in the inset, with atoms P, C1, C2, and C3 labelled. (B) Two-dimensional plot of $\nabla^2\rho$ (X2C-PBE0-D3BJ/x2c-TZVPPall//r^{2}SCAN-3c) of **TS** in the P–C1–C2 plane; bond paths are shown as black lines, (3, –1) critical points are shown as black circles, positive contour lines are shown as blue solid lines, and negative contour lines are shown as red dashed lines. (C) Surface plots (PBE0-D3BJ/def2-TZVP//r^{2}SCAN-3c) (isovalue = 0.06) depicting overlap between the C1-centered vacant p-orbital and a filled P–C3 NBO (*left*) and overlap between a filled C1-centered lone pair and the P–C3 σ* NBO (*right*). Further details are provided in the ESI.

orbital at C1 to afford an energy of stabilization of 57.9 kcal/mol (Figure 6C). Additionally, the lone pair at C1 delocalizes into the P–C3 σ* orbital to afford an energy of stabilization of 50.6 kcal/mol (Figure 6C).

These computational data collectively suggest that the formation of **8** from **7** and CO proceeds through a concerted mechanism in which coordination of the CO unit to the P center results in the breaking of the PC_2 ring, in agreement with previous results.[1d] Topological and NBO analyses of **TS** suggest that the P–C3 bond is cleaved prior to the breaking of the P–C2, whilst the P–C1 bond can still be considered dative in nature.

Open Access Article. Published on 29 April 2026. Downloaded on 4/30/2026 5:17:44 AM.
This article is licensed under a Creative Commons Attribution 3.0 Unported Licence.

Dalton Transactions Accepted Manuscript

Please do not adjust margins

Conclusions

In summary, we have investigated sterically encumbered phosphanides in the activation of N_2O, CO_2, and CO. Efforts to expand the reactivity patterns reported herein to catalytic processes involving these small molecules are currently underway.

Author contributions

J.S.W.: Conceptualization, data curation, funding acquisition, investigation, methodology, visualization, writing–original draft, writing–review and editing. W.J.R.: Investigation, writing–review and editing. M.M.: Conceptualization, funding acquisition, project administration, resources, supervision, writing–review and editing.

Conflicts of interest

There are no conflicts to declare.

Data availability

The data supporting this article have been included as part of the Supplementary Information. Crystallographic data for **4**, **5**, ^{13}**6**, **7**•(toluene)$_{0.5}$, and ^{13}**8** have been deposited *via* the joint CCDC/FIZ Karlsruhe deposition service under 2537504, 2537507, 2537506, 2537503, and 2537505, respectively.

Acknowledgements

We thank the UKRI for funding (EP/Y037391/1) and supporting M.M. We thank the ERC for funding a Marie Skłodowska-Curie Fellowship (101205172) and supporting J.S.W. We are also grateful to the University of Oxford for computing resources.

Notes and references

1. (a) L. Liu, D. A. Ruiz, D. Munz and G. Bertrand, *Chem*, 2016, **1**(*1*), 147–153; (b) M. M. Hansmann, R. Jazzar and G. Bertrand, *J. Am. Chem. Soc.*, 2016, **138**(*27*), 8356–8359; (c) M. M. Hansmann and G. Bertrand, *J. Am. Chem. Soc.*, 2016, **138**(*49*), 15885–15888; (d) Y. Chen, P. Su, D. Wang, Z. Ke and G. Tan, *Nat. Commun.*, 2024, **15**, 4579; (e) T. G. Saint-Denis, T. A. Wheeler, Q. Chen, G. Balázs, N. S. Settineri, M. Scheer and T. D. Tilley, *J. Am. Chem. Soc.*, 2024, **146**(*7*), 4369–4374.
2. A. Genoux, T. H. Wong, F. Fadaei-Tirani and K. Severin, *Chem. Commun.*, 2025, **61**(*80*), 15654–15657.
3. (a) W. Rundel and P. Kästner, *Justus Liebigs Ann. Chem.*, 1964, **686**(*1*), 88–91; (b) N. Szynkiewicz, J. Chojnacki and R. Grubba, *Inorg. Chem.*, 2020, **59**(*9*), 6332–6337; (c) D. Dhara, P. K. Pal, R. Dolai, N. Chrysochos, H. Rawat, B. J. Elvers, I. Krummenacher, H. Braunschweig, C. Schulzke, V. Chandrasekhar, U. D. Priyakumar and A. Jana, *Chem. Commun.*, 2021, **57**(*75*), 9546–9549; (d) M. Jörges, S. Mondal, M. Kumar, P. Duari, F. Krischer, J. Löffler and V. H. Gessner, *Organometallics*, 2024, **43**(*4*), 585–593; (e) R. J. Ward, M. Jörges, H. Remm, E. Kiliani, F. Krischer, Q. Le Dé and V. H. Gessner, *J. Am. Chem. Soc.*, 2024, **146**(*35*), 24602–24608; (f) T. Koike, J.-K. Yu and M. M. Hansmann, *Science*, 2024, **385**(*6706*), 305–311; (g) Y. Mei, X.-Y. He, J. Li, M. Liu, Q. Liang, C. Yang and L. L. Liu, *Nat. Commun.*, 2025, **16**, 2321.
4. D. W. Stephan and G. Erker, *Chem. Sci.*, 2014, **5**(*7*), 2625–2641.
5. (a) R. Appel, B. Laubach and M. Siray, *Tetrahedron Lett.*, 1984, **25**(*39*), 4447–4448; (b) T. Taeufer, F. Dankert, D. Michalik, J. Pospech, J. Bresien and C. Hering-Junghans, *Chem. Sci.*, 2023, **14**(*11*), 3018–3023; (c) J. M. Goicoechea and H. Grützmacher, *Angew. Chem., Int. Ed.*, 2018, **57**(*52*), 16968–16994.
6. S. Fujimori and S. Inoue, *J. Am. Chem. Soc.*, 2022, **144**(*5*), 2034–2050.
7. (a) M. Wu, H. Li, W. Chen, D. Wang, Y. He, L. Xu, S. Ye and G. Tan, *Chem*, 2023, **9**(*9*), 2573–2584; (b) D. Wang, C. Zhai, Y. Chen, Y. He, X.-D. Chen, S. Wang, L. Zhao, G. Frenking, X. Wang and G. Tan, *Nat. Chem.*, 2023, **15**(*2*), 200–205; (c) X. Wang, Y. Chen, X. Li, L. Xu and G. Tan, *J. Am. Chem. Soc.*, 2025, **147**(*41*), 36980–36986; (d) G. Tan and S. Ye, *Acc. Chem. Res.*, 2025, **59**(*3*), 397–410.
8. J. S. Wenger, N. Gaschik, W. J. Rowe, A. E. Crumpton, B. van IJzendoorn and M. Mehta, *Chem. Sci.*, 2026, **17**, 7475–7485.
9. V. L. Rudzevich, H. Gornitzka, K. Miqueu, J.-M. Sotiropoulos, G. Pfister-Guillouzo, V. D. Romanenko and G. Bertrand, *Angew. Chem., Int. Ed.*, 2002, **41**(*7*), 1193–1195.
10. N. Yoza, N. Ueda and S. Nakashima, *Fresenius' J. Anal. Chem.*, 1994, **348**(*10*), 633–638.
11. R. F. W. Bader, *Chem. Rev.*, 1991, **91**, 893–928.

View Article Online DOI: 10.1039/D6DT00966J

Open Access Article. Published on 29 April 2026. Downloaded on 4/30/2026 5:17:44 AM. This article is licensed under a Creative Commons Attribution 3.0 Unported Licence.

Dalton Transactions Accepted Manuscript

This journal is © The Royal Society of Chemistry 20xx

View Article Online
DOI: 10.1039/D6DT00986G

The data supporting this article have been included as part of the Supplementary Information. Crystallographic data for **4**, **5**, ^{13}**6**, **7**•(toluene)$_{0.5}$, and ^{13}**8** have been deposited *via* the joint CCDC/FIZ Karlsruhe deposition service under 2537504, 2537507, 2537506, 2537503, and 2537505, respectively.

Open Access Article. Published on 29 April 2026. Downloaded on 4/30/2026 5:17:44 AM.
This article is licensed under a Creative Commons Attribution 3.0 Unported Licence.

Dalton Transactions Accepted Manuscript